JMEPEG (2008) 17:802–807
DOI: 10.1007/s11665-008-9226-4
©ASM International
1059-9495/$19.00

Simulation and Analysis of Residual Stress in the Graded Interlayer of $MoSi_2$ Composite/316L Stainless Steel Joint

Jinfu Xu, Haifei Wu, Xuebin Zhang, Youjin Fei, Yifu Ye, and Wen Li

(Submitted March 21, 2007; in revised form November 22, 2007)

We reported the simulation and the analysis of the residual stress within the graded interlayered joints of $MoSi_2$ to 316L stainless steel fabricated by spark plasma-sintering (SPS) technique. The residual stress in the joints was analyzed by the finite element ANSYS code. The results show that the maximum radial and axial residual tension stresses first decrease and then increase with the increase of the compositional distribution exponent (*P*), and consistently decrease with the increase of the number (*n*) and the thickness (*d*) of graded layer, respectively. The optimal values of compositional distribution exponent, the thickness, and the number of graded interlayered joints of the $MoSi_2$ composite/316L are $P = 0.8$, $d = 1.0$ mm, and $n = 9$, respectively. The residual tension stresses in the samples treated by nine graded interlayers are reduced to 24% and 25% of those in the joints without the interlayer, respectively.

Keywords graded interlayer, joining, molybdenum disilicide, residual stress, spark plasma sintering (SPS), 316L stainless steel

1. Introduction

Molybdenum disilicide ($MoSi_2$) is being developed as a potential high-temperature structural material because of its high melting point (T_m = 2030 °C), moderate density, excellent oxidation resistance, good electrical conductivity, and stability in a variety of corrosive environments (Ref 1, 2). Many potential applications have been identified for $MoSi_2$ in the aerospace industry, automotive industry, energy sources, and so on (Ref 3, 4).

For using $MoSi_2$ in various industries, it must first be joined to other materials, such as ferrous and nonferrous alloys. However, direct bonding of $MoSi_2$ to most metals and alloys is not possible owing to differences in coefficient of thermal expansion (CTE) and the necessity for high joining temperatures, which can lead to joint failure upon cooling because of large residual stresses. To solve this tough problem, various welding/joining techniques have been employed. For example, Conzone et al. (Ref 5) first used active brazing techniques to obtain the tense uniformed joints of $MoSi_2$ to 316L. However, the Cu/Si phase produced at the $MoSi_2$/Nb interface limits the temperature used for $MoSi_2$/316L joints because it has a relatively low melting temperature (852 °C), and successful use of this joint at temperatures approaching 852 °C could only be achieved in a nonoxidizing environment.

In a previous work, we had developed a new approach of spark-plasma sintering (SPS) by the use of 9 graded interlayers made of $MoSi_2$ and 316L with different compositions to join $MoSi_2$ composite and 316L stainless steel. A joint with excellent properties was achieved at moderate temperatures. However, the residual thermal stress induced during cooling, which is the key issue in the joining strength within the graded interlayer, cannot be effectively and accurately measured by x-ray and other common methods (as the graded interlayer has nine layers and $MoSi_2$ is an intermetallic compound). In this work, the influence of compositional distribution exponent, thickness, and number of the graded interlayer on the value and distribution of residual thermal stress simulated by the finite element ANSYS code were investigated.

Jinfu Xu, Haifei Wu, and **Yifu Ye**, Institute of Material Science & Engineering, East China University of Science and Technology, Shanghai 200237, China; **Jinfu Xu**, Research Institute of Material and Technology, Ningbo University of Technology, Ningbo 315016, China; **Xuebin Zhang** and **Youjin Fei**, Institute of Material Science & Engineering, China University of Mining and Technology, Xuzhou 221008, China; and **Wen Li**, Key Laboratory of Low Dimensional Materials and Application Technology (Ministry of Education), Faculty of Materials and Optoelectronic Physics, Xiangtan University, Xiangtan, Hunan 411105, China. Contact e-mail: wenl@ualberta.ca.

2. Analysis Model

2.1 Geometrical Model and Boundary Condition

A geometrical model for joints was established, based on the following assumptions to simplify the model and benefit the analysis of the residual stress in the grade interlayer: no change in the material properties at high temperatures, no plastic deformation in the joint during cooling, and layers bonding each other tightly. The parameters of thermophysical properties are isotropy and irrelevant to the change of temperature. Besides, the geometrical model for joints takes a cylindrical shape with 20 mm diameter, as shown in Fig. 1. The intersection point between the central axis and the bottom surface is chosen as the origin of coordinate. Half of the longitudinal surface is selected for the analysis of the residual stress because of the symmetry. The sample is separated into $n + 2$ layers along the *Y*-axis and the bottom layer is pure 316L stainless

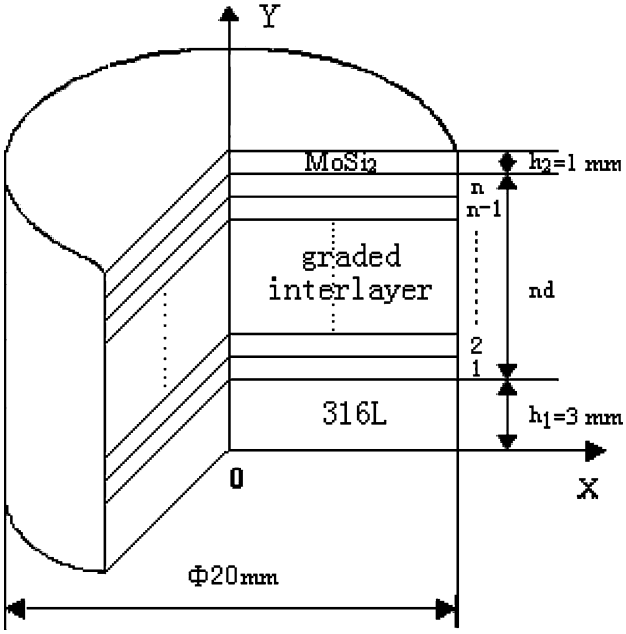

Fig. 1 A joint with graded interlayer

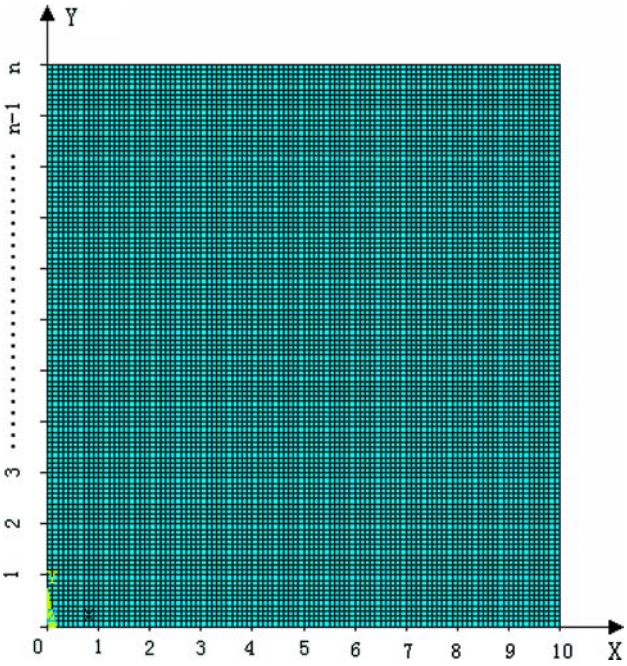

Fig. 2 Finite element analysis model of $MoSi_2$/316L joint

steel with a thickness of 3.0 mm. The top layer is $MoSi_2$ composite (containing 10 at% ZrO_2 to improve the toughness of $MoSi_2$) with a thickness of 1.0 mm. The graded interlayer is in the central part of the sample and d refers the thickness of each graded interlayer. A rectangular axial symmetric element is selected by dividing half of the cross section of the model by finite element mesh. There are 100 elements in the radial and axial directions, 30 elements in the 316L layer, 10 elements in the $MoSi_2$ layer, and $10 \times d$ elements in each graded layer as shown in Fig. 2. The shape of the graphite die for sintering the joints by SPS is schematically shown in Fig. 3, which maintains

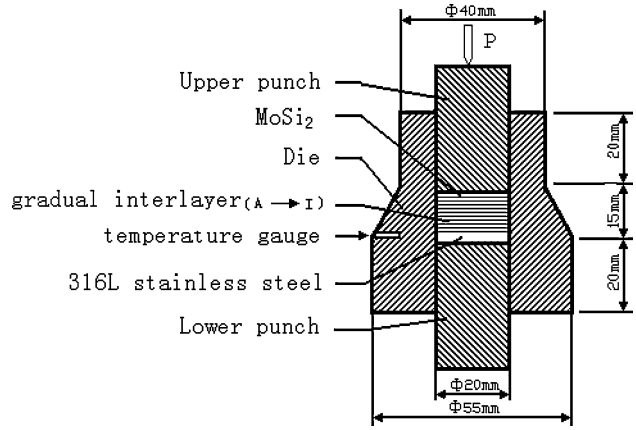

Fig. 3 The graphite die used for SPS

Table 1 Mechanical and physical properties of $MoSi_2$ and 316L

Materials	*E*, GPa	CTEs, $\alpha/(10^{-6}/°C)$	*K*, W/(m °C)	*v*	σ_f, MPa
$MoSi_2$	420	8.1	25	0.3	560
316L	193	16	16.3	0.3	1120
ZrO_2	151	10.0	2.09	0.33	150

250 °C temperature difference between the upper and the lower end of the die (Ref 6). Then, the boundary conditions can be given as following: the lower and upper boundaries are set as 1200 °C and $[1200 + 250/15 \times (4 + n \times d)]$ °C, respectively. The displacement of *Y*-axis along the direction of *X* is 0 because of the fixed origin of coordinate. The other boundaries are set to be free.

2.2 Model of Physical Parameters

The physical properties of materials are listed in Table 1 (Ref 7, 8). The composition of the graded interlayer can be described as the power function (Ref 9):

$$C_i = \left(\frac{y-3}{n \times d}\right)^P, 0 \le y \le n \times d, 1 \le i \le n \quad \text{(Eq 1)}$$

where C_i is the volume fraction of the (i)th layer of $MoSi_2$ and y is the distance from the midline point of the (i)th graded interlayer to the zero point in *Y*-axis. Here, $y = 3 + (i-0.5) \times d$, where n is the number of layer, d is the thickness of each graded interlayer, and P is the compositional distribution exponent, respectively.

Here, the coefficient of thermal expansion α (CTE), Poisson's ratio v, and heat transfer coefficient K of the linear compound can be expressed as (Ref 10):

$$\begin{aligned} \alpha &= C_1\alpha_1 + C_2\alpha_2; \\ v &= C_1 v_1 + C_2 v_2; \\ \kappa &= C_1\kappa_1 + C_2\kappa_2; \end{aligned} \quad \text{(Eq 2)}$$

where subscripts 1 and 2 represent $MoSi_2$ and 316L stainless steel, respectively; and C_1 and C_2 are the volume fractions of $MoSi_2$ and 316L in the graded material ($C_1 + C_2 = 1$), respectively.

The elastic modulus E can be found by (Ref 11):

$$E = \left(C_1 E_1 \frac{q + E_2}{q + E_1} + C_2 E_2\right) \Big/ \left(C_1 \frac{q + E_2}{q + E_1} + C_2\right) \qquad \text{(Eq 3)}$$

where E_1 and E_2 are the elastic moduli of $MoSi_2$ and 316L, respectively; and q is the empirical constant, which is ~4500 MPa.

3. Results and Discussions

3.1 Influence of Compositional Exponent (P) on Residual Stress

Setting $d = 1.0$ mm and $n = 9$, the relationship between residual stress and compositional distribution exponent (P) is shown in Fig. 4. It suggests that the radial (X) maximum tensile stress and the axial (Y) maximum tensile stress in the joint first decrease and then increase with the increase of the compositional exponent, and reach the lowest point when $P = 1.0$ and $P = 0.6$, respectively. Because the CTE plays a key role in the generation of residual stress, it is necessary to study the influence of compositional exponent P on the CTEs of the graded interlayer, as shown in Fig. 5. When P is 0.5 and 1.5, the CTEs of the materials for sintering joints display a rather large mismatch, which would result in a large thermal residual stress; whereas, when P is 0.8, the CTEs match closely with those of 316L and $MoSi_2$, which would result in a low residual stress obtained in the joints.

The major factor causing the $MoSi_2$ crack (perpendicular to the surface) is the radial (X) tension stress, while that in the interlayers is the axial (Y) tension stress (Ref 12). Here, the range from 0.6 to 1.0 is initially selected as the value of P according to the principle of minimum stress.

The ability to bear tension stress in the 316L side is significantly higher than in the $MoSi_2$ composite. So, during the design of the composition of the graded interlayer, the center position of maximum residual tension stress should approach the region with a high content of 316L as much as possible, which can be accomplished by adjusting the compositional distribution exponent (P). The relationship between the center position of maximum axial residual tension stress in Y-axis and the compositional distribution exponent (P) is shown in Fig. 6.

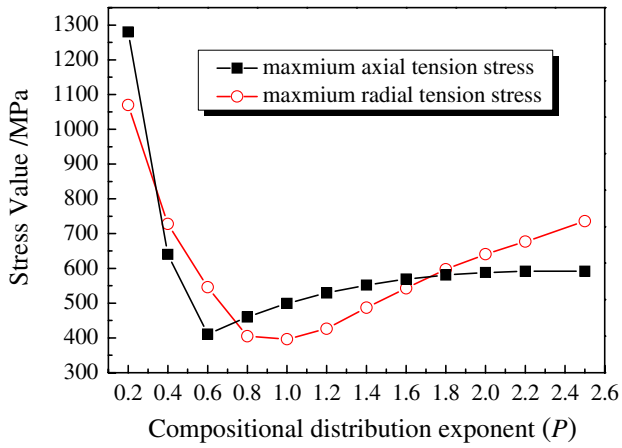

Fig. 4 Variation of maximum residual tension stress with compositional distribution exponent (P)

It shows the center position of maximum residual tension stress shifts from the side with more 316L to that with more $MoSi_2$ with the increase of the compositional exponent (P). The value of Y is almost equal to 11.2 when P varies from 0.6 to 2.5, which suggests that the position of maximum axial residual tension stress is in the ninth layer approaching the $MoSi_2$ side. However, the value of Y is <5.2 when P varies from 0.2 to 0.4, and the position of maximum axial residual tension stress is located between the first and the third layer of the graded interlayer, approaching the 316L side. To obtain the minimum thermal stress, the value range of P from 0.6 to 1.0 is initially elected.

With the increase of P, the change of physical parameters in the graded interlayer is the major factor to cause the shift of the center position of the maximum axial tension stress, which results in the maximum different region of physical parameters in the graded interlayer shifting to the side with more $MoSi_2$. Because the thermal residual stress is mainly generated in the nonhomogeneous temperature field, the distribution of thermal residual stress is mainly affected by the physical parameters and the gradient temperature field. Thus, the center position of

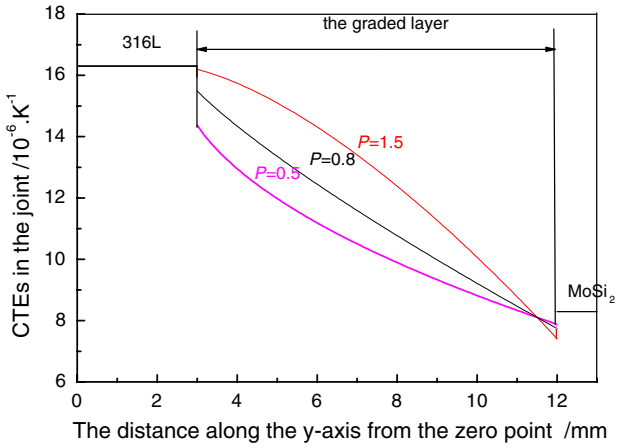

Fig. 5 Variation of CTEs of the graded layer with compositional distribution exponent (P)

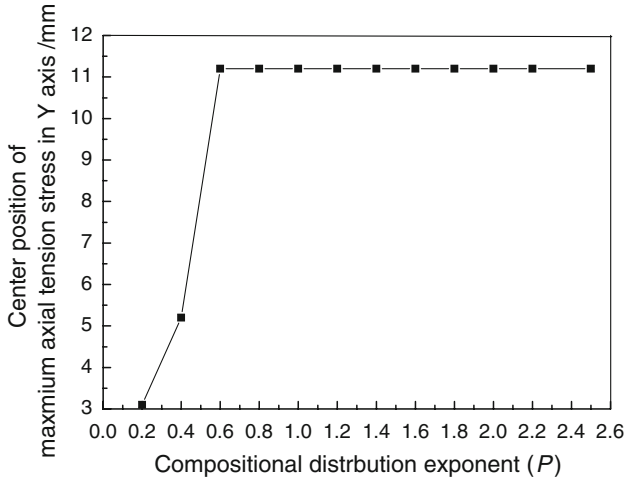

Fig. 6 Relationship between center positions of maximum axial residual tension stress with compositional distribution exponent (P)

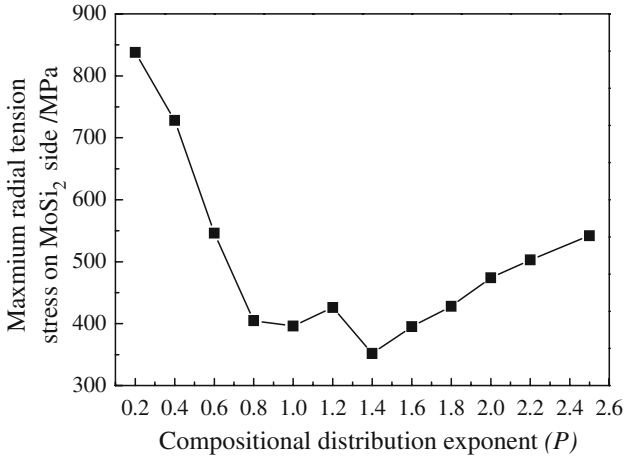

Fig. 7 Variation of maximum radial tension stress of $MoSi_2$ side with compositional distribution exponent (P)

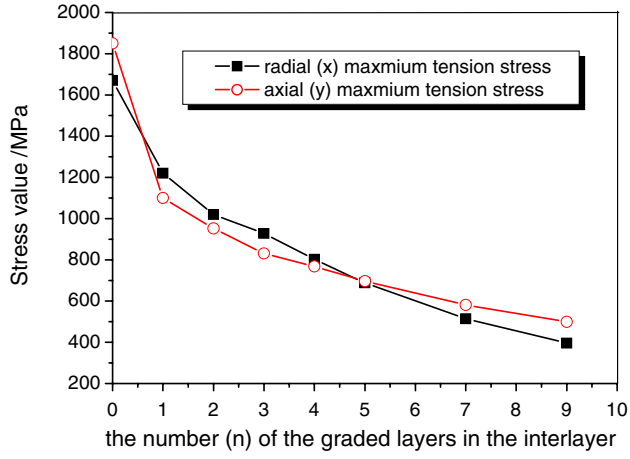

Fig. 8 Variation of maximum tension stress with number (n) of the graded layers in the interlayer

maximum residual tension stress shifts from the side with more 316L to that with more $MoSi_2$.

The weakest part of the joints during cooling and in the following applications is always found in the $MoSi_2$ composite side. To examine the minimum thermal stress and its original position, the influence of residual stress on the $MoSi_2$ composite side should be further studied. The relation between maximum radial tension stress of the $MoSi_2$ composite side and compositional distribution exponent (P) is plotted in Fig. 7. It is clearly implied that the value of maximum radial tension stress of the $MoSi_2$ composite side first decreases sharply and then increases slowly with the increase of P, and reaches the minimum when the value of P is up to 1.4.

Based on this discussion, $P = 0.8$ is selected as the optimal value of compositional exponent to make the maximum axial and radial tension stresses of joints simultaneously reach the minimum value and the maximum radial tension stress in the $MoSi_2$ composite side.

3.2 Influence of Number (n) of Graded Layers on Residual Stress

The relationship between maximum tension stress and number (n) of the graded layers is shown in Fig. 8 when P and d are set as 0.8 and 1.0 mm, respectively. It clearly shows that the maximum tension stress in the axial and radial directions decreases with the increase of n. The larger the value of n is, the more homogeneous the compositional transition is. The slower the change of physical parameters is, the more the reduction of interface stress concentration is, and the trend becomes smooth when n is up to 9. Compared with the noninterlayer joint, the maximum axial and radial tension stresses with nine graded layers are reduced to 24% and 25% of those in the noninterlayer joint, respectively, which is lower than the fracture strength of $MoSi_2$ (560 MPa). Here, $n = 9$ in the design of the graded structure, which could effectively relax the thermal stress.

3.3 Influence of Thickness (d) of Each Graded Layer in the Interlayer on Residual Stress

The relationship between maximum tension stress and thickness (d) of each layer in the interlayer is shown in Fig. 9

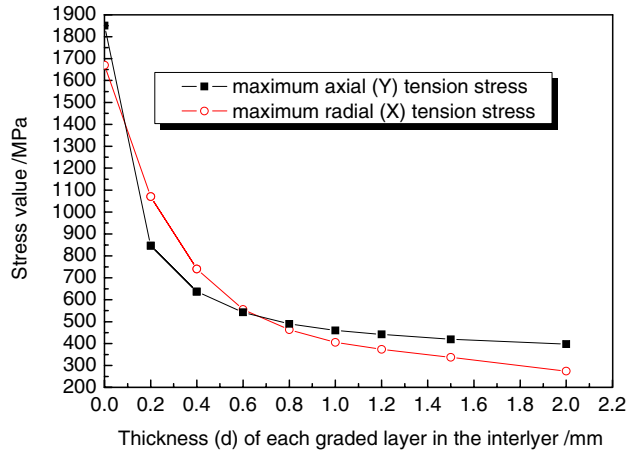

Fig. 9 Variation of maximum tension stress with thickness (d) of each graded layer in the interlayer

when P and n are set as 0.8 and 9, respectively. It suggests that the maximum axial and radial tension stresses decrease with the increase of d. The maximum axial and radial tension stresses with the nine grade layers are reduced to 24% and 25% of those in noninterlayer joint when d is 1.0 mm. It shows that the graded layers could effectively reduce the thermal stress. When d is lower than 0.6 mm, the maximum tension stress, especially the maximum radial tension stress, sharply changes with the increase of d; however, when d is more than 1.0 mm, the trend turns smooth, and there is no great change in the maximum axial tension stress. Herein, $d = 1.0$ mm for the sintering of the joints.

4. Results and Discussions

4.1 Sintering of Joint

According to the results of analysis, the 316L/$MoSi_2$ composite joint is sintered with 98.0% pure $MoSi_2$ (<10 μm), 99% pure ZrO_2 (40 μm), 98% pure 316L (165 μm) powder that

Table 2 Volume fraction of $MoSi_2$/316L graded interlayers

Layer	316L stainless steel powder	$MoSi_2$ powder
A	90.10	9.90
B	76.15	23.85
C	64.11	35.89
D	53.03	46.97
E	42.57	57.43
F	32.56	67.44
G	22.92	77.08
H	13.57	86.43
I	4.47	95.53

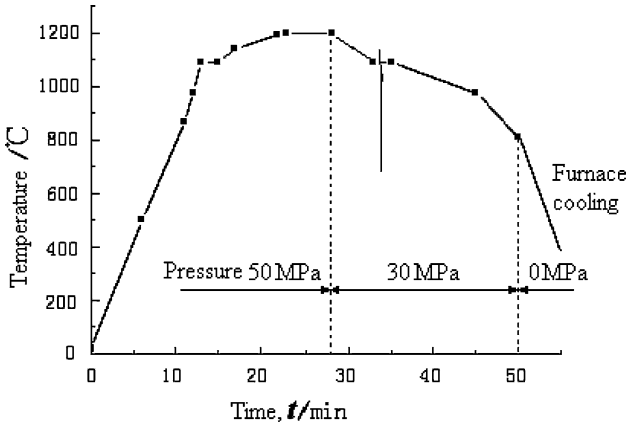

Fig. 10 Sintering process of SPS

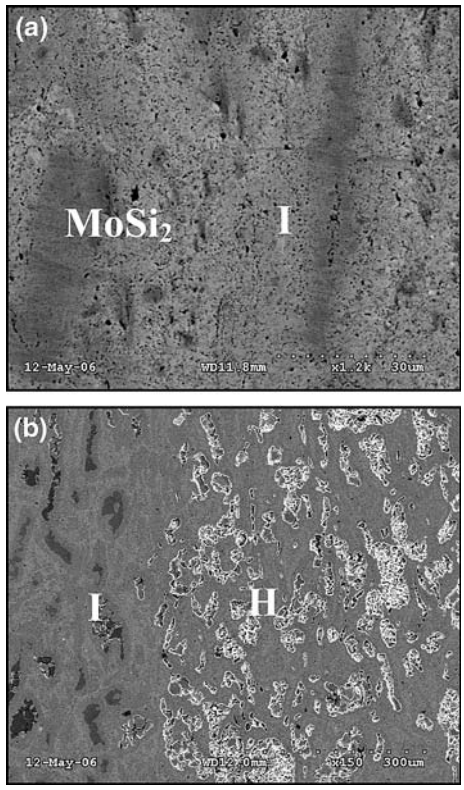

Fig. 12 A typical SEM image for the $MoSi_2$/316L joint. The marked I and H are the I and H layer as labeled in Fig. 10

are obtained commercially. The composition of the graded interlayer is shown in Table 2. Powders of each layer are mixed by in agate ball-grinding cans in a planetary ball miller (QM-SB) for 4 h. Then, the obtained powder mixtures are cold-pressed layer by layer in a graphite die (Fig. 3). The layers of the powders are arranged in the following sequence: 316L, A, B, C, D, E, F, G, H, I, J, K, $MoSi_2$ composite (containing 10% ZrO_2 to improve the fracture toughness). The thickness of each layer is 1 mm except the layer of 316L pressed to be 3 mm, followed by pre-press under the pressure of 6 MPa. Then the sample is sintered in a SPS system (Dr. SINTER, SPS-1030, Sumitomo Coal Mining Co. Ltd., Japan) with the sintering parameters shown in Fig. 10.

4.2 Microstructural Observations

The specimens after sintering are sliced off along the longitudinal section and the microstructure of the interface is examined by a scanning electron microscope (SEM S250 MK3) and an optical microscope. The metallurgical morphology of a joint is shown in Fig. 11. As shown in Fig. 11, the microstructure of the joint is arranged at 316L/A/B/…/I/10% ZrO_2–$MoSi_2$ from left to right, and the interfaces between layers are not clear markedly, indicating that the composition of layers is changed slowly and the interfaces are bonding well. It is also seen that the graded interlayer produced a joint without microcracks or porosities. Some interface microstructures of the joints are shown in Fig. 12(a) and (b). According to the finite element analysis of the residual stress discussed above, there should be a rather large value of axial tension stress in the ninth layer of the graded interlayer. However, as shown in Fig. 12(a), there is no macro-deficiency and crack in the interface of $MoSi_2$-I and I-H. Meanwhile, there should be a rather large value of radial tension stress in the $MoSi_2$ side, however, no cracks are observed vertical to the surface of $MoSi_2$, as shown in the

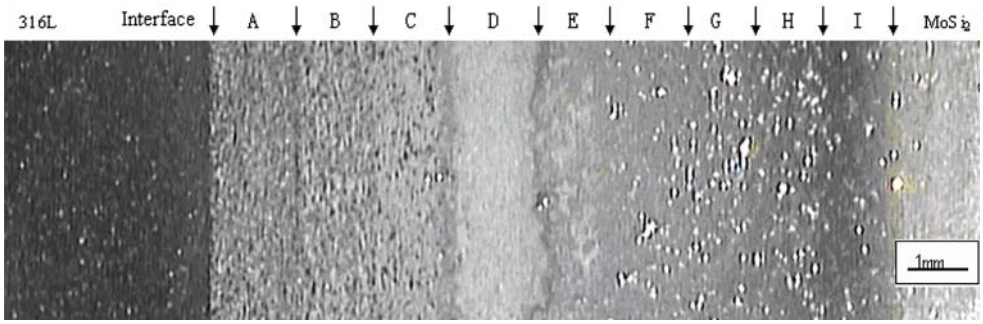

Fig. 11 A typical optical microstructural image of the $MoSi_2$/316L joint

Fig. 12(b). These results suggest the interfaces between each layer bond tightly.

5. Discussion

As shown in Fig. 11 and 12, the sharp interlayer boundaries disappeared because of interdiffusion that not only changed the boundary conditions stipulated in the model but also altered the physical and mechanical properties of the interlayers. In our simulation, the calculation of the thermal stress of the $MoSi_2$ composite/316L joint is based on two phases of $MoSi_2$ and 316L, and their elastic deformation during the cooling process from sintering temperature to room temperature. In fact, plastic deformation and low-speed creep deformation might appear in 316L stainless steel, and the slow interdiffusion might occur in $MoSi_2$ at high temperatures, which could relax the thermal stress during the cooling process of the sintered samples and cause the theoretical value of thermal stress to be larger than the actual value in the sintered samples. Here, the design for the $MoSi_2$/316L joint present in this paper is credible when the stress is considered only.

6. Conclusions

A model for the design of $MoSi_2$ composite/316L joints is proposed. The relationships between the compositional distribution exponent P and residual stress, graded layer number n and residual stress, the thickness of graded layer d, and residual stress are accomplished via the finite element ANSYS code. Results show that the optimal compositional distribution exponent, the thickness, and the number of the graded interlayer are $P = 0.8$, $d = 1.0$ mm, $n = 9$ for the fabrication of $MoSi_2$/316L joint, respectively. A compact uniformed joint with each layer bonding tightly within the interlayer was obtained by the SPS sintering technology according to the simulated results, which suggests the current work provides a facile and helpful method for the sintering of the $MoSi_2$/316L joint.

References

1. J. Kuchino, K. Kurokawa, and T. Shibayama, et al., Effect of Microstructure on Oxidation Resistance of $MoSi_2$ Fabricated by Spark Plasma Sintering, *Vacuum*, 2004, **73**, p 623–628
2. P.V. Krakhmalev, E. Strom, and C. Li, Microstructure and Properties Stability of Al-Alloyed MoSi2 Matrix Composites, *Intermetallics*, 2004, **12**, p 225–233
3. A.K. Vasudeval and J.J. Petrovic, A Comparative Overview of Molybdenum Disilicide Composites, *Mater. Sci. Eng.*, 1992, **A155**, p 2–3
4. J.J. Petrovic, Mechanical Behavior of MoSi2 and MoSi2 Composites, *Mater. Sci. Eng. A*, 1995, **A192/A193**, p 31–37
5. S.D. Conzone, D.P. Butt, and A.H. Bartlett, Joining MoSi2 to 316L Stainless Steel, *J. Mater. Sci.*, 1997, **32**, p 3369–3374
6. M. Shinichi and T. Masato. Homogenization of Functionally Graded Materials (FGM) by Spark Plasma Sintering (SPS)[C]//NEDO International Symposium on FGM, 1999, p 183–186
7. R.U. Vaidya, Y.P. Rangaswam, and M.A. M Bourke, et al., Measurement of Bulk Residual Stresses in Molybdenum Disilicide/Stainless Steel Joints Using Neutron Scattering, *Acta Mater.*, 1998, **46**(6), p 2047–2061
8. Y.J. Xu, D.H. Tu, and X.M. Li, Steady Thermal Stress of Functionally Gradient Material Plate Under Convective Heat Transfer Boundary, *Mater. Mech. Eng.*, 2004, **28**(7), p 15–17
9. L.J. Zhang, Q.H. Rao, and Y.H. He, et al., Research Advance on Thermal Stress of Functionally Gradient Materials, *Mater. Sci. Eng. Powder Metall.*, 2005, **10**(5), p 257–262
10. Y. Zhang, N.S. Liu, and L.Q. Chen, et al., Determination of the Physical Properties of Functional Gradient Materials, *J. Solid Rocket Technol.*, 2004, **27**(1), p 77–80
11. X.H. Zhang, W. Qu, and X.Z. Zhang, et al., Optimum Design of TiC-Ni Functionally Graded Materials, *Mater. Sci. Tech.*, 2000, **8**(1), p 81–83
12. X.H. Zhang, J.C. Han, and B.L. Wang, et al., Combustion Synthesis and Thermal Stress Analysis TiC-NiFGM, *J. Astronautics*, 2001, **22**(1), p 89–94